JOURNAL OF MATERIALS SCIENCE **38** (2003) 2135–2141

Carbon-nanofibre-reinforced poly(ether ether ketone) fibres

J. SANDLER, A. H. WINDLE
Department of Materials Science and Metallurgy, University of Cambridge, Cambridge CB2 3QZ, UK
E-mail: msps100@cam.ac.uk

P. WERNER
Lehmann & Voss & Co., D-22043 Hamburg, Germany

V. ALTSTÄDT
Department of Polymer Engineering, University of Bayreuth, D-95440 Bayreuth, Germany

M. V. ES
DSM Research, 6160 MD Geleen, The Netherlands

M. S. P. SHAFFER*
Department of Chemistry, Imperial College London, South Kensington Campus, London SW7 2A2, UK
E-mail: m.shaffer@imperial.ac.uk

Nano-reinforced fibres were spun from a semicrystalline high-performance poly(ether ether ketone) containing up to 10 wt% vapour-grown carbon nanofibres using conventional polymer processing equipment. Mechanical tensile testing revealed increases in nanocomposite stiffness, yield stress, and fracture strength for both as-spun and heat-treated fibres. X-ray and differential scanning calorimetry analyses were performed in order to investigate both the orientation of nanofibres within the polymer matrix and the matrix morphology. The carbon nanofibres were found to be well aligned with the direction of flow during processing. Significantly, the degree of crystallinity of the poly(ether ether ketone) matrix was found to increase with the initial addition of nanofibres although the crystal structure was not affected. The measured increase in composite tensile modulus is compared to injection-moulded nanocomposite samples made from the same blends. The results highlight the need to characterise the matrix morphology when evaluating nanocomposite performance and hence deducing the intrinsic properties of the nanoscale reinforcement.

1. Introduction

The development of carbon-nanotube and carbon-nanofibre-reinforced polymer composites not only offers unique opportunities to improve the physical and mechanical properties of a given matrix but also allows the evaluation of the intrinsic properties of the reinforcing nanoscale phase. The use of carbon nanotubes and vapour-grown carbon nanofibres as reinforcements has already been shown to improve the mechanical properties of various polymer matrix systems (for a recent review on carbon-nanotube-based polymer composites see [1] and the references therein) [2–6]. Standard polymer processing can often be used satisfactorily for these nanocomposites and does not break down the reinforcement material, an issue commonly encountered in short-fibre-composites which can limit recyclability. Furthermore, initial studies have indicated that the small size of the nanoscale reinforcement allows an enhancement of the properties of delicate structures such as polymer fibres [7, 8].

The key technical challenges which remain for such carbon-nanotube and nanofibre-reinforced polymers are the achievement of a homogeneous dispersion, good interfacial bonding and a controlled degree of alignment. It is also apparent from these studies that an ability to predict nanocomposite properties for a given filler type and loading fraction remains challenging, with different increases in performance being reported for different types of nanostructures. Depending on the type of reinforcement, additional factors such as the crystalline quality [9] as well as the 'waviness' of the fibrous filler inside the matrix are expected to influence the reinforcement capability [10].

Current approaches towards increasing the orientation of the nanoscale reinforcement within the polymer matrix range from optimisation of the extrusion

* Author to whom all correspondence should be addressed.

die [5] to stretching the composite melt to form fibres [7, 8, 11]. In addition, changes in the morphology of semicrystalline thermoplastic polymers due to the presence of carbon nanotubes and nanofibres have been observed [3, 12, 13]. Processing techniques that lead to oriented polymers can induce different crystallisation behaviours, but the effects of carbon nanotubes or nanofibres on such oriented polymer systems, although significant [13], have not yet been fully established. Interactions of the nanoscale reinforcement with the matrix during processing and the resulting effects on overall composite performance need to be considered when attempting to evaluate the intrinsic properties of the reinforcement.

In a recent study [6] we showed that twin-screw extrusion and injection-moulding successfully led to the production of nanocomposites containing well-dispersed and aligned vapour-grown carbon nanofibres in a high-performance semicrystalline poly(ether ether ketone) (PEEK) matrix with improved mechanical properties. The addition of nanofibres in concentrations up to 15 wt% resulted in a linear increase with concentration in composite tensile modulus, yield stress and fracture strength, while matrix ductility was maintained up to loading fractions of 10 wt%. Differential scanning calorimetry (DSC) indicated that for this matrix system the nanofibres did not alter the polymer morphology under the applied processing conditions. Nevertheless, we provided evidence that the presence of nanofibres could influence the matrix morphology under certain conditions. The nanofibres did not act as a nucleation site for crystallisation, which started in the bulk of the polymer, but, on slow cooling from the melt, the surface structure of the nanofibres led to an enhanced secondary crystallisation in the confined space between and around the nanofibres [6].

The present study was aimed at investigating the potential of vapour-grown carbon nanofibres as a reinforcement for poly(ether ether ketone) melt-spun nanocomposite fibres. The application of such a melt-spinning process was expected to lead to improved alignment of the nanoscale reinforcement within the matrix. The influence of the nanofibre content on the mechanical performance of the composite fibres was characterised by tensile tests for both as-spun and heat-treated samples. DSC and X-ray diffraction were applied to investigate the crystalline structure and the degree of crystallinity of the matrix, as well as the degree of alignment of the reinforcement.

2. Materials and experimental details

Poly(ether ether ketone) powder, grade Victrex 450G, was obtained from ICI. The vapour-grown carbon nanofibres (CNF) [Pyrograf III PR-19-PS] were purchased from Applied Sciences Inc, USA. The carbon nanofibre material consists of a mixture of two distinctive structures present in the sample, relatively straight cylindrical tubes and the so-called bamboo tube-like structures, arranged into loose aggregates. The inner part of a nanofibre wall, for both tubes and bamboo-like structures, shows an arrangement of the graphitic layers at a $\pm 15^\circ$ angle with respect to the fibre axis. The outside part of the wall is made up of short graphitic segments parallel to the fibre axis. The nanofibre material has an aspect (length-to-diameter) ratio of around 1000 in the as-received state and is free of carbonaceous contaminations.

PEEK nanocomposite masterbatches containing 0, 5 and 10 wt% CNF were prepared using a Berstorff co-rotating twin-screw extruder with a length-to-diameter ratio of 33. From these masterbatches, carbon-nanofibre-reinforced PEEK fibres were spun from a Rheometrics Scientific capillary rheometer at 370°C with a drawing speed of about 15 m/min. This process resulted in an average fibre diameter of 0.19 ± 0.02 mm. A set of samples was subsequently heat-treated at 200°C for 30 min, followed by 4 hrs at 220°C, an approach previously used for injection-moulded carbon-nanofibre-reinforced PEEK composites in order to maximise crystallinity [6]. Field emission gun scanning electron microscopy (FEGSEM) was carried out on gold-coated, liquid nitrogen fracture surfaces of the fibre specimens, using a JEOL 6340F.

Force-controlled fibre tensile tests were performed at room temperature with a TA Instrument 2980 Dynamic Mechanical Analyser. The fibres with a gauge length of 5.5 mm were gripped in thin film tension clamps. Stress-strain curves up to specimen fracture were obtained for all materials by ramping the force up at 0.1 N/min. DSC was performed on fibre bundles using Perkin Elmer equipment. Melting and crystallisation patterns were recorded at 10°C/min during heating and cooling measurements between 70 and 380°C .

X-ray fibre diffraction patterns of both the as-spun and the heat-treated samples were collected, at room temperature, on a CCD array, using a Ni-filtered Cu K_α source, operating at 40 kV and 30 mA, calibrated with silicon powder. The diffraction pattern of the vapour-grown carbon nanofibres is dominated by a strong Bragg peak centred around 0.34 nm, which corresponds to the interlayer spacing within the nanofibres (referred to as the (002) peak hereafter). The slightly larger d spacing as compared to graphite is related to the stacking disorder in these nanostructures. Due to the internal 'herringbone' arrangement of the graphitic planes (oriented at $\pm 15^\circ$ with respect to the tube axis) the (002) reflection tends to appear as a small arc instead of a sharp peak even for perfectly aligned nanofibres.

3. Results and discussion

SEM images of fracture surfaces of two PEEK nanocomposite fibres are shown in Fig. 1. The image on the left is an as-spun composite fibre containing 5 wt% and the one on the right is a heat-treated nanocomposite fibre containing 10 wt% carbon nanofibres. Both images reveal the homogeneous dispersion of carbon nanofibres within the matrix. No nanofibre agglomerates or voids could be observed in any of the fibres investigated. The images indicate both a high degree of alignment of the nanofibres to the spinning direction and a high quality surface finish.

Fig. 2 shows comparative stress-strain diagrams of the (a) as-spun and (b) heat-treated PEEK nanocomposite fibres as a function of nanofibre weight fraction.

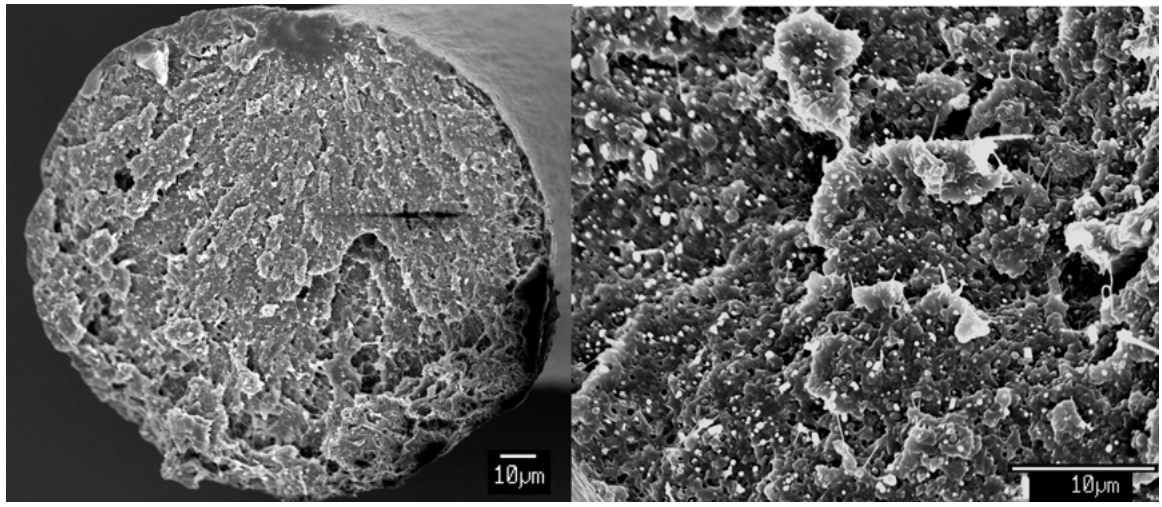

Figure 1 Scanning electron micrographs of fracture surfaces of (left) an as-spun nanocomposite fibre containing 5 wt% and (right) a heat-treated nanocomposite fibre containing 10 wt% carbon nanofibres, showing the homogeneous dispersion and alignment of nanofibres achieved during processing.

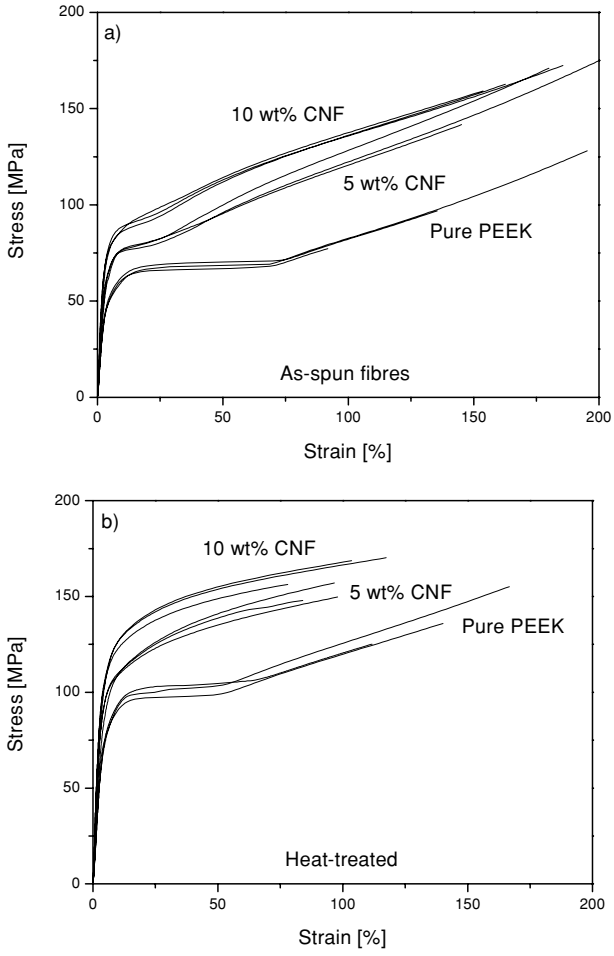

Figure 2 Representative stress-strain diagrams of the composite fibres as a function of nanofibre loading. Curves displayed are for (a) the as-spun fibres and (b) the heat-treated samples.

At least three fibres were tested for each loading fraction and only minor deviations in mechanical properties such as modulus and yield stress were observed. The deviations in strength and strain to failure for a given set of samples can be attributed to the experimental method used. As can be seen there is an increase in tensile modulus for both types of material with increasing nanofibre weight fraction. The as-spun nanocomposite fibres revealed an initial yielding at about 3% strain, followed by uniform necking and drawing. (It is important to note that the tensile test was based on a constant force ramp and not on a constant crosshead displacement speed and thus no 'yield drops' were observed.) The pure PEEK matrix showed such a necking plateau up to about 70% strain before strain-induced crystallisation and subsequent stiffening occurred. The plateau region before the strain-hardening was significantly reduced for the as-spun nanocomposites containing 5 wt% nanofibres and hardly present for the sample containing 10 wt%. The fibre fracture strength appears to increase with the addition of nanofibres for the as-spun samples whereas the strain to failure does not seem affected within experimental accuracy. After heat-treatment, there was a general improvement in modulus, yield stress, and fracture strength whereas the ultimate elongation was reduced for the two nanocomposites. The heat-treated samples displayed a necking plateau for the pure matrix only, which retained a yield strain of about 20% but strain-hardening occurred earlier at about 50%.

The microstructure of PEEK, in terms of crystallite morphology and orientation, is dependent on its thermal history and the manufacturing process employed [14], as well as the presence of possible nucleation sites [15]. In carbon-fibre-reinforced PEEK, the presence of macroscopic fibres and variations in their surface microstructure were found to additionally influence matrix morphology [16–18]. Subsequent heat-treatment of such composites also influences the matrix morphology [19]. Therefore, in this study, DSC analysis was performed on all samples in order to assess the crystal structure and the degree of crystallinity.

On heating the as-spun nanocomposite fibres in the DSC, the PEEK glass transition, T_g, at 143°C, was followed by a clear exotherm, centred at 163°C, representing a continuation of the crystallisation process that was suppressed by quenching the fibres after spinning. This crystallisation feature was shifted to higher temperatures by 20–25°C for the pure PEEK matrix although the glass transition was indistinct. For all of

TABLE I DSC thermal parameters recorded for PEEK-CNF nanocomposite fibre samples during heating. All calculated degrees of crystallinity X_c are normalised to the actual weight fraction of polymer. For comparison, the degree of crystallinity determined from the X-ray analysis is also included

Processing		As-spun			Heat-treated (30 min @ 200°C + 4 h @ 220°C)		
Analysis		PEEK	5 wt%	10 wt%	PEEK	5 wt%	10 wt%
DSC	T_g (°C)	–	143	143	–	–	–
	T_r (°C)	182	162	162	–	–	–
	T_m (°C)	332	332	332	328	328	328
	X_c (%)	6	12	12	13	18	19
X-ray	X_c (%)	6	8	10	13	17	20

The theoretical value for the enthalpy of melting for 100% crystalline PEEK was taken to be 130 J/g [14].

the as-spun fibres, continued heating revealed a melting feature at 300–330°C with a shape characteristic of the combined recrystallisation and melting associated with small crystallites. After heat-treatment, both fibre and injection-moulded samples showed only a single melting peak at around 330°C [6], with no evidence for either earlier crystallisation or recrystallisation during melting.

The positions of the glass transition, crystallisation, and melting features are summarised in Table I. Evaluation of the enthalpies normalised to the actual weight fraction of polymer present, allowed the determination of the degree of crystallinity X_c achieved during fibre processing. As can be seen from Table I, X_c of the pure as-spun PEEK fibres was about 6% and increased to 12% for both untreated nanocomposite fibres. The heat-treated pure PEEK fibre had a degree of crystallinity of 13% which increased to about 18% for both treated nanocomposite fibres.

The results from the DSC analysis clearly showed that, in the case of melt-spun PEEK nanocomposite fibres, the presence of the nanoscale reinforcement led to an increase in the overall degree of crystallinity. This increase was present in both types of fibres but appears to be independent of nanofibre content. On the other hand, the melting peak, which is related to the crystallite thickness and the distribution of spherulite size, gave no indication of any change in crystallite structure. A sharp onset to melting occurred at 295°C and was independent of nanofibre content and heat-treatment.

Complimentary evidence for these effects was provided by the X-ray analysis. Fig. 3 shows typical 2-D diffraction patterns of the as-spun and heat-treated pure PEEK fibres and the 10 wt% nanocomposite fibres. The 2-D pattern of the as-spun pure PEEK fibre in Fig. 3a reveals a broad ring from the diffuse scattering of the polymer matrix. With increasing nanofibre addition, the increase in crystallinity becomes evident (b). On the other hand, Fig. 3c clearly shows the increase in crystallinity for the pure PEEK fibres with heat-treatment. Again, the presence of carbon nanofibres further increased the overall degree of crystallinity in this system (d).

The alignment of the nanofibres is demonstrated by the arcs of the (002) Bragg reflection, indicated by the arrows in Fig. 3. Azimuthal scans for both the as-spun and the heat-treated nanocomposite fibres indicate that the graphitic layers are aligned to within approximately $\pm 30°$. Taking into account the crystallographic arrangement of the graphitic planes in these nanofibres, which are partly arranged in a 'herringbone' structure, the degree of alignment of the nanofibres can be considered to be even higher. This alignment is independent of nanofibre content and was not observed to change significantly during heat-treatment.

Equatorial scans of the diffraction patterns also clearly revealed the increase in crystallinity with both nanofibre content and heat-treatment. Fig. 4 shows an intensity vs 2θ plot for the as-spun pure PEEK and the 10 wt% composite fibre and all the heat-treated PEEK composite fibres. The intensities are normalised with regard to the amorphous background. The polymer main reflexions in this plot are labelled (110), (200), (111), and (211) and correspond to the so-called crystal I form of PEEK [20]. This two-chain orthorhombic crystal structure has been previously observed for melt-spun and annealed PEEK monofilaments [20]. As can be seen from the (110) peak intensity, the degree of crystallinity is improved for the nanocomposite fibres compared to the pure PEEK fibres but this increase is independent of nanofibre content, in agreement with the DSC data. The degrees of crystallinity were estimated from the approximate relative areas under the amorphous and crystalline peaks, and are listed in Table I for comparison with the DSC results.

These trends in crystallinity are useful for understanding the mechanical properties, as discussed below, but their origins are not completely straightforward to interpret. The essential phenomenon is that all of the spun fibres have a much lower crystallinity than injection-moulded and subsequently heat-treated samples made from the same masterbatches. One likely interpretation is that a combination of rapid quenching with a high degree of polymer alignment induced by the spinning process produces a distribution of very small crystallites in the pure fibre matrix. Alignment of the polymer was indicated by both strong birefringence of the fibres and the alignment of the crystallites in the X-ray patterns, whilst the presence of small crystallites is suggested by the shape of the melting peak observed in the DSC. Such small crystallites have been found previously to constrain PEEK and increase its T_g [21, 22], and may prevent maximum crystallisation after annealing above T_g. For the injection-moulded samples, slower cooling from the melt allowed larger crystals to grow as evidenced by a higher melting peak

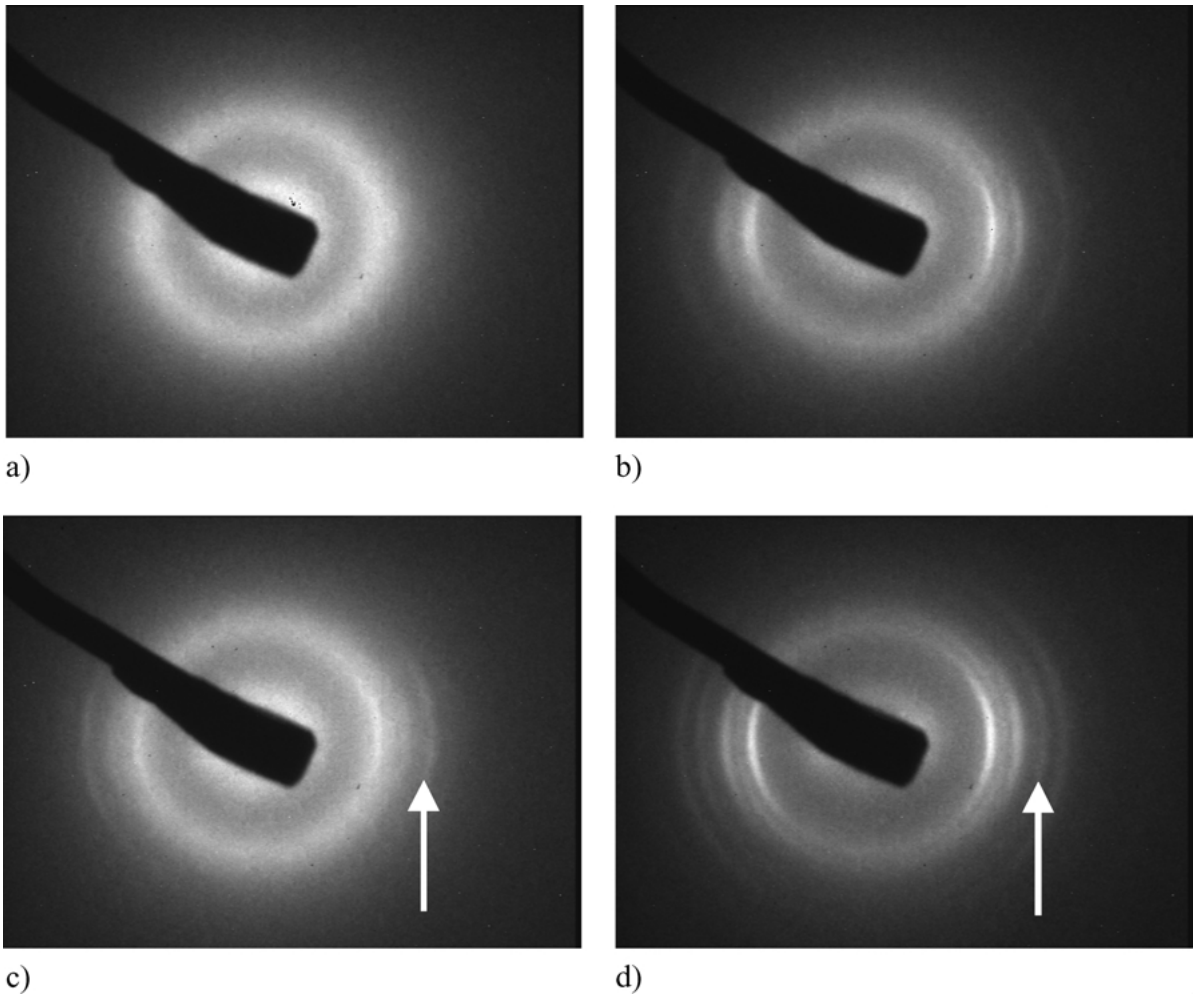

Figure 3 X-ray fibre diffraction patterns of (a) as-spun and (b) heat-treated pure PEEK fibres, (c) as-spun, and (d) heat-treated nanocomposite fibres containing 10 wt% carbon nanofibres.

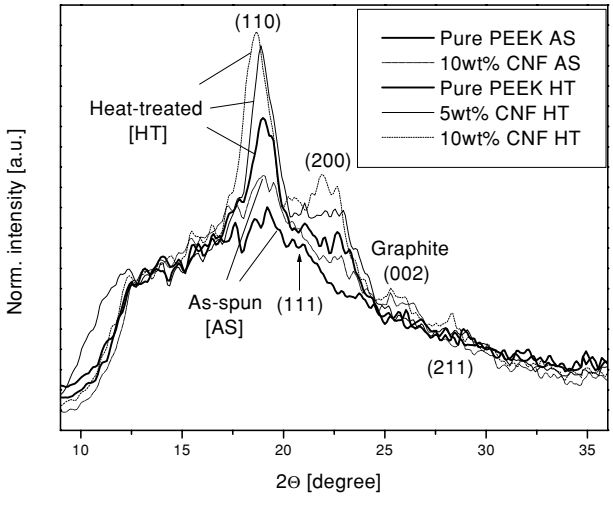

Figure 4 Normalised equatorial intensities (from Fig. 3) as a function of 2θ for as-spun and heat-treated pure PEEK and nanocomposite fibres, showing the increase in crystallinity with heat-treatment and carbon nanofibre addition.

temperature, a normal bulk T_g and the normal maximum crystallinity attained after heat-treatment [6]. On adding the nanofibres, the crystallinity of the fibres all but doubles, although the absolute value remains relatively low. The nanofibres also reduce the temperature at which crystallisation occurs on heating in the DSC. The nanofibres must play some sort of nucleating role in the development of crystallinity of this oriented system, although a loading of 10 wt% of nanofibres has little additional influence over 5 wt%. Given that the nanofibres did not appear to act as nucleating agents in the injection-moulded samples [6], the effect is probably related to local changes in polymer orientation or strain, caused by the presence of the nanofibres during the spinning process, rather than to direct surface heteronucleation. However, further work will be required to elucidate the mechanism in detail.

Since the mechanical properties of a semicrystalline polymer depend on the crystal structure and especially the degree of crystallinity, these effects need to be taken into account when evaluating nanocomposite performance. Fig. 5 shows the composite fibre tensile modulus as a function of nanofibre loading for both the as-spun and heat-treated samples. As a reference, the composite moduli for injection-moulded and heat-treated nanocomposites prepared from the same masterbatches are included [6]. The solid line for the injection-moulded samples is a linear fit to the experimental data. The numerical labels refer to the degrees of crystallinity as obtained from the DSC measurements. As can be seen, both sets of fibres show an enhanced initial increase in modulus with the addition of 5 wt% nanofibres compared to the injection-moulded samples.

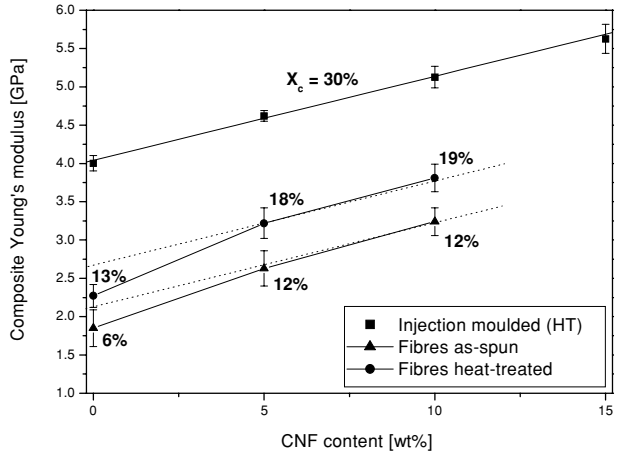

Figure 5 Young's modulus of as-spun and heat-treated PEEK composite fibres as a function of nanofibre weight fraction. Data for injection-moulded PEEK nanocomposites from [6] is included for comparison. The data labels refer to the degree of crystallinity as determined from DSC measurements. The solid lines are included as visual aids and the dashed lines lie parallel to the linear increase in composite modulus observed for the injection-moulded samples.

This enhancement is associated with the extra crystallinity resulting from the presence of the nanofibres. Further addition of nanofibres to the polymer fibres does not alter the crystallinity, but leads to an increase in modulus which matches the increase observed for the injection-moulded samples.

Taking into account the variations in crystallinity of these nanocomposites, the further improvement in mechanical performance of these systems can be straightforwardly ascribed to conventional reinforcement effects of the carbon nanofibres. Following Krenchel's expression for short carbon fibre composites (Equation 1) [23], where E_f and E_m are the fibre and matrix moduli, and η_0 and η_1 are efficiency factors relating to the orientation and length of the fibres, respectively:

$$E = \eta_0 \eta_1 V_f E_f + (1 - V_f) E_m \qquad (1)$$

and averaging over all nanocomposite samples, the effective nanofibre modulus $\eta_0 \eta_1 E_f$ is about 22 GPa. This effective modulus is lower than the value of about 100 GPa that can be estimated from the work by Kumar *et al.* for carbon-nanofibre-reinforced polypropylene fibres [8]. However, it has been established that the carbon nanofibres act as polymer nucleation sites in polypropylene [3]. Such a change in morphology of oriented polypropylene [13], which was not taken into account in reference [8], might explain the higher effective nanofibre modulus observed.

Considering the degree of alignment observed in our study and taking an estimate for the effective aspect ratio of the carbon nanofibres, short-fibre theory predicts an intrinsic nanofibre modulus of around 100 GPa. The low intrinsic modulus of the vapour-grown carbon nanofibres can be attributed to their defective graphitic structure in the outer part of the walls.

Although it can be argued that, here, the nanofibres have only improved laboratory-spun PEEK fibres and that the intrinsic properties of the polymer could be improved by suitable drawing and thermal treatments, this study shows that the resulting nanocomposite characteristics arise from the combination of the matrix and nanofiller properties. Hence, even with improved matrix crystallinity and alignment, the introduction of nanofibres would be expected to yield additional increases in stiffness and strength. Note that commercial PEEK fibres have a stiffness around 6 GPa [24], which is significantly less than the effective modulus of the nanofibres observed in these experiments and substantially less than the likely effective modulus of high-crystallinity nanotubes. In addition, the presence of the nanofibres increases the melt-strength of the polymer [25] and hence allows the spinning of finer PEEK filaments which are a current focus of interest.

4. Conclusion

This study has shown that vapour-grown carbon nanofibres can be used as a nanoscale reinforcement for delicate polymer structures such as fibres. Twin-screw extrusion of a semicrystalline poly(ether ether ketone) matrix and carbon nanofibres led to masterbatches that were subsequently processed into nanocomposite fibres. The addition of nanofibre weight fractions up to 10 wt% was not detrimental to either the ease of processing or to the fibre surface finish. The polymer nanocomposite fibres exhibited a homogeneous dispersion and excellent alignment of the nanoscale reinforcement. The addition of carbon nanofibres was shown clearly to increase mechanical properties such as modulus, yield stress and fracture strength. Furthermore, changes in the degree of matrix crystallinity due to the nucleating properties of the nanoscale reinforcement were revealed by DSC and X-ray analysis. The improvements in the mechanical properties of the nanocomposite fibres were attributed to a combination of the increase in crystallinity and the reinforcing effects of the filler. This study highlights the need to characterise matrix morphology prior to evaluation of nanocomposite or nanoreinforcement performance.

Acknowledgements

J. Sandler wishes to acknowledge financial support from the EC Thematic Network 'CNT-Net' [G5RT-CT-2001-05026], the EPSRC and the Cambridge European Trust. The authors would like to thank the National Centre for Biomedical Engineering Science in Ireland for use of their experimental equipment.

Volker Altstädt would like to take this opportunity to commemorate the 65th birthday of Prof. Dr.-Ing. Dr. h.c. G.W. Ehrenstein.

References

1. E. T. THOSTENSON, Z. REN and T.-W. CHOU, *Comp. Sci. Tech.* **61** (2001) 1899.
2. O. S. CARNEIRO, J. A. COVAS, C. A. BERNADO, G. CALDEIRA, F. W. J. VAN HATTUM, J.-M. TING, R. L. ALIG and M. L. LAKE, *ibid.* **58** (1998) 401.
3. K. LOZANO and E. V. BARRERA, *J. Appl. Polym. Sci.* **79** (2001) 125.

4. C. A. COOPER, D. RAVICH, D. LIPS, J. MAYER and H. D. WAGNER, *Comp. Sci. Tech.* **62** (2002) 1105.
5. R. J. KURIGER, M. K. ALAM, D. P. ANDERSON and R. L. JACOBSEN, *Composites* Part A **33** (2002) 53.
6. J. SANDLER, P. WERNER, M. S. P. SHAFFER, V. DEMCHUK, V. ALTSTÄDT and A. H. WINDLE, *ibid.* **33** (2002) 1033.
7. R. HAGGENMUELLER, H. H. GOMMANS, A. G. RINZLER, J. E. FISCHER and K. I. WINEY, *Chem. Phys. Lett.* **330** (2000) 219.
8. S. KUMAR, H. DOSHI, M. SRINIVASARAO, J. O. PARK and D. A. SCHIRALDI, *Polymer* **43** (2002) 1701.
9. J.-P. SALVETAT, A. J. KULIK, J.-M. BONARD, G. A. D. BRIGGS, T. STÖCKLI, K. MÉTÉNIER, S. BONNAMY, F. B. BÉGUIN, N. A. BURNHAM and L. FORRÓ, *Adv. Mater.* **11** (1999) 161.
10. F. T. FISHER, R. D. BRADSHAW and L. C. BRINSON, *Appl. Phys. Lett.* **80** (2002) 4647.
11. M. SENNETT, E. WELSH, J. B. WRIGHT, W. Z. LI, J. G. WEN and Z. F. REN, *Mater. Res. Soc. Symp. Proc.* **706** (2002) Z3.31.
12. B. P. GRADY, F. POMPEO, R. L. SHAMBAUGH and D. E. RESASCO, *J. Phys. Chem.* B **106** (2002) 5852.
13. J. SANDLER, G. BROZA, M. NOLTE, K. SCHULTE, Y.-M. LAM and M. S. P. SHAFFER, *J. Macromol. Sci.-Phys. Ed.* (2002) in press.
14. D. J. BLUNDELL and B. N. OSBORN, *Polymer* **24** (1983) 953.
15. C. Y. BARLOW, J. A. PEACOCK and A. H. WINDLE, *Composites* **21** (1990) 383.
16. R. A. CRICK, D. C. LEACH, P. J. MEAKIN and D. R. MOORE, *J. Mater. Sci.* **22** (1987) 2094.
17. T. Q. LI, M. Q. ZHANG, K. ZHANG and H. M. ZHENG, *Polymer* **41** (2000) 161.
18. T. Q. LI, M. Q. ZHANG and H. M. ZHENG, *Composites* Part A **32** (2001) 1727.
19. P.-Y. JAR, W. J. CANTWELL and H. H. KAUSCH, *Comp. Sci. Tech.* **43** (1992) 299.
20. T. LIU, S. WANG, Z. MO and H. ZHANG, *J. Appl. Polym. Sci.* **73** (1999) 237.
21. J. R. ATKINSON, J. N. HAY and M. J. JENKINS, *Polymer* **43** (2002) 731.
22. D. A. IVANOV, R. LEGRAS and A. M. JONAS, *Macromolecules* **32** (1999) 1582.
23. D. HULL, "An Introduction to Composite Materials" (Cambridge University Press, Cambridge, 1981) p. 95.
24. Personal communication with Zyex Ltd., www.zyex.co.uk
25. P. WERNER *et al.* (2002) in preparation.

Received 15 August
and accepted 11 November 2002